

Design and fabrication of MEMS devices using the integration of MUMPs, trench-refilled molding, DRIE and bulk silicon etching processes

Mingching Wu and Weileun Fang

Department of Power Mechanical Engineering, National Tsing Hua University, Hsinchu, Taiwan

E-mail: fang@pme.nthu.edu.tw

Received 17 August 2004

Published DD MMM 2004

Online at stacks.iop.org/JMM/15/1

Abstract

This work integrates multi-depth DRIE etching, trench-refilled molding, two poly-Si layers MUMPs and bulk releasing to improve the variety and performance of MEMS devices. In summary, the present fabrication process, named MOSBE II, has three merits. *First*, this process can monolithically fabricate and integrate poly-Si thin-film structures with different thicknesses and stiffnesses, such as the flexible spring and the stiff mirror plate. *Second*, the multi-depth structures, such as vertical comb electrodes, are available from the DRIE processes. *Third*, a cavity under the micromachined device is provided by the bulk silicon etching process, so that a large out-of-plane motion is allowed. In application, the optical scanner driven by self-aligned vertical comb actuator was demonstrated. The poly-Si micromachined components fabricated by the MOSBE II can further integrate with the MUMPs devices to establish a more powerful MOEMS platform.

(Some figures in this article are in colour only in the electronic version)

1. Introduction

It is difficult to fabricate complicated three-dimensional MOEMS (micro-opto-electro-mechanical systems) structures using the planar micromachining fabrication processes. These thin-film processes also restrict the mechanical characteristics, such as the stiffness, of the micromachined structures. Meanwhile, the variety of MEMS devices is limited. Similar to their macroscopic counterpart, the micromachined mechanisms and devices are usually consisted of components with different mechanical characteristics. For instance, the micro-optical scanner consisting of a flexible torsional spring and a stiff mirror is preferred [1, 2]. Consequently, various complicated fabrication processes have been presented to fabricate and to integrate micromachined components with different mechanical characteristics [3–5].

The MUMPs process is regarded as one of the most popular fabrication technology for MOEMS. However, the

performances of these surface micromachined devices are limited to the thickness of the thin-film materials. For instance, the stiffness of the micromachined structures such as the mirror plate and the supporting beam are too low to tolerate the thin-film residual stresses [6]. The MOSBE (molded surface-micromachining and bulk etch release) process [7, 8] has employed the bulk silicon etching to tune the cross-section shape of a thin-film structure, so as to increase its stiffness. Integrating the flexible thin-film structure with the stiff bulk silicon component using the bonding process is presented in [8, 9]. As a second example, the thickness of thin film also limits the moving space of the surface micromachined MUMPs devices [3]. In [10, 11], the cantilever bent by residual stress has been exploited to lift up the MUMPs scanner, so as to increase its scanning angle. The idea of using micro actuator to lift up MUMPs devices is realized in [12]. The bulk silicon etching is used in the hybrid MOSBE process [7] to increase

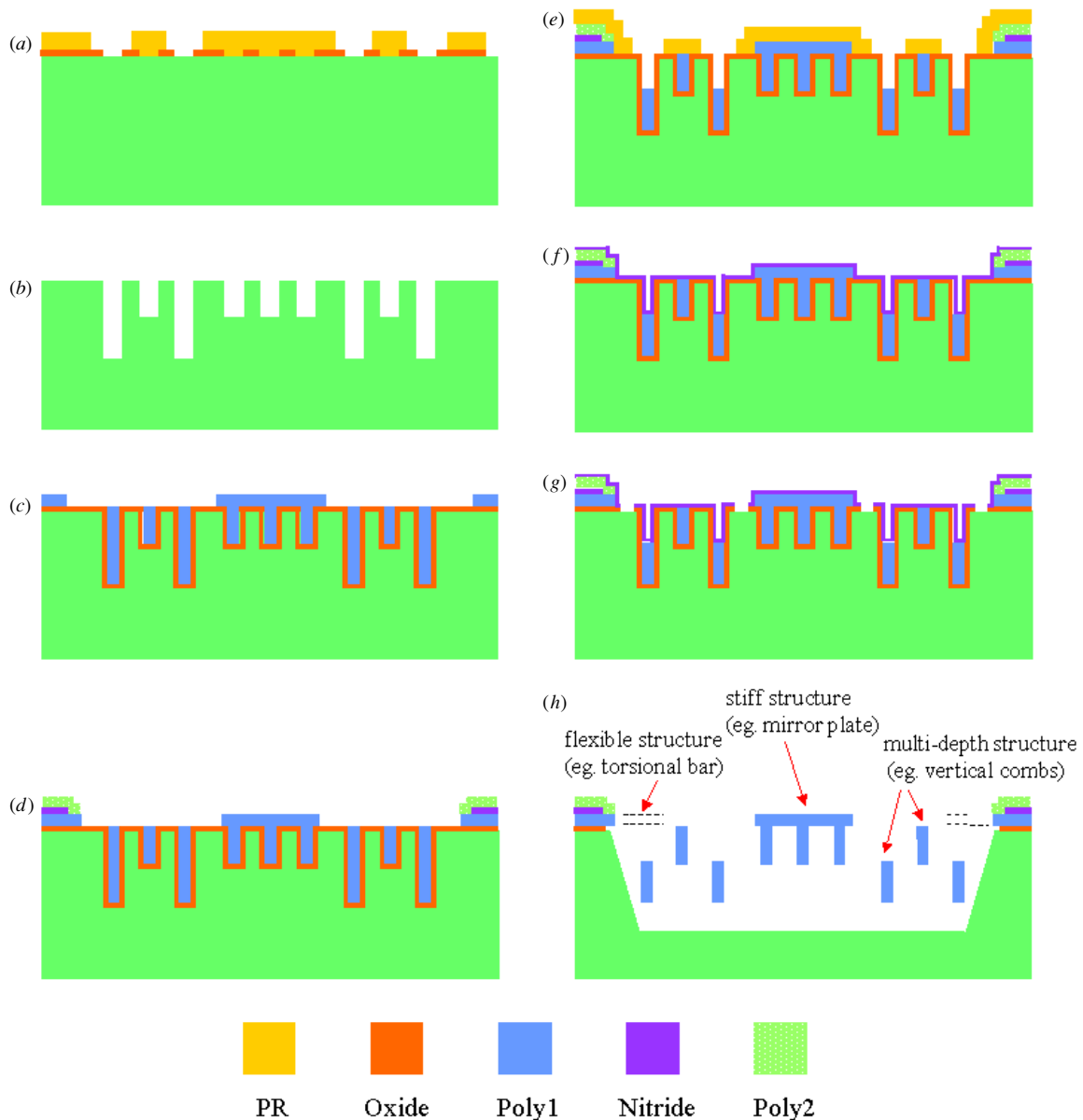


Figure 1. The detailed fabrication process steps.

the space between the surface micromachined components and the substrate. In this case, the surface micromachined components are made of silicon nitride instead of poly silicon thin film to survive after bulk silicon etching. Thus, the components of MOSBE cannot integrate with the devices of the well-established MUMPs process. Because Si_xN_y is dielectric material, the device in [8] suffers from the electrical routing problem.

The goal of this work is to establish a novel fabrication process named MOSBE II to integrate the DRIE (deep reactive ion etching), trench-refilled molding [13, 14], two poly-Si MUMPs and bulk silicon etching. The present MOSBE II processes have three merits. *First*, this process can monolithically fabricate and integrate poly-Si thin film structures with different thicknesses and stiffnesses, such as the flexible spring and the stiff mirror plate. *Second*, the multi-depth structures, such as vertical comb electrodes, are available from the DRIE processes. *Third*, a cavity under the micromachined device is provided by the bulk silicon etching

processes, so that a large out-of-plane motion is allowed. Thus the variety and performance of micromachined devices can be significantly improved.

2. Fabrication processes

The fabrication processes present in this study are illustrated in figure 1. As shown in figures 1(a) and (b), the DRIE was employed to provide trenches with various depths on the silicon substrate. The processes in figures 1(c)–(g) were the deposition, patterning and stacking of thin films. These processes were similar to the concept of surface micromachining, however, the idea of trench-refill molding was employed to form thick and multi-depth structures. As shown in figure 1(h), the micromachined structures were fully released and suspended after the bulk silicon etching and the removing of sacrificial thin films.

The processes began with the deposition and patterning of thermal oxide. A second photolithography was used to

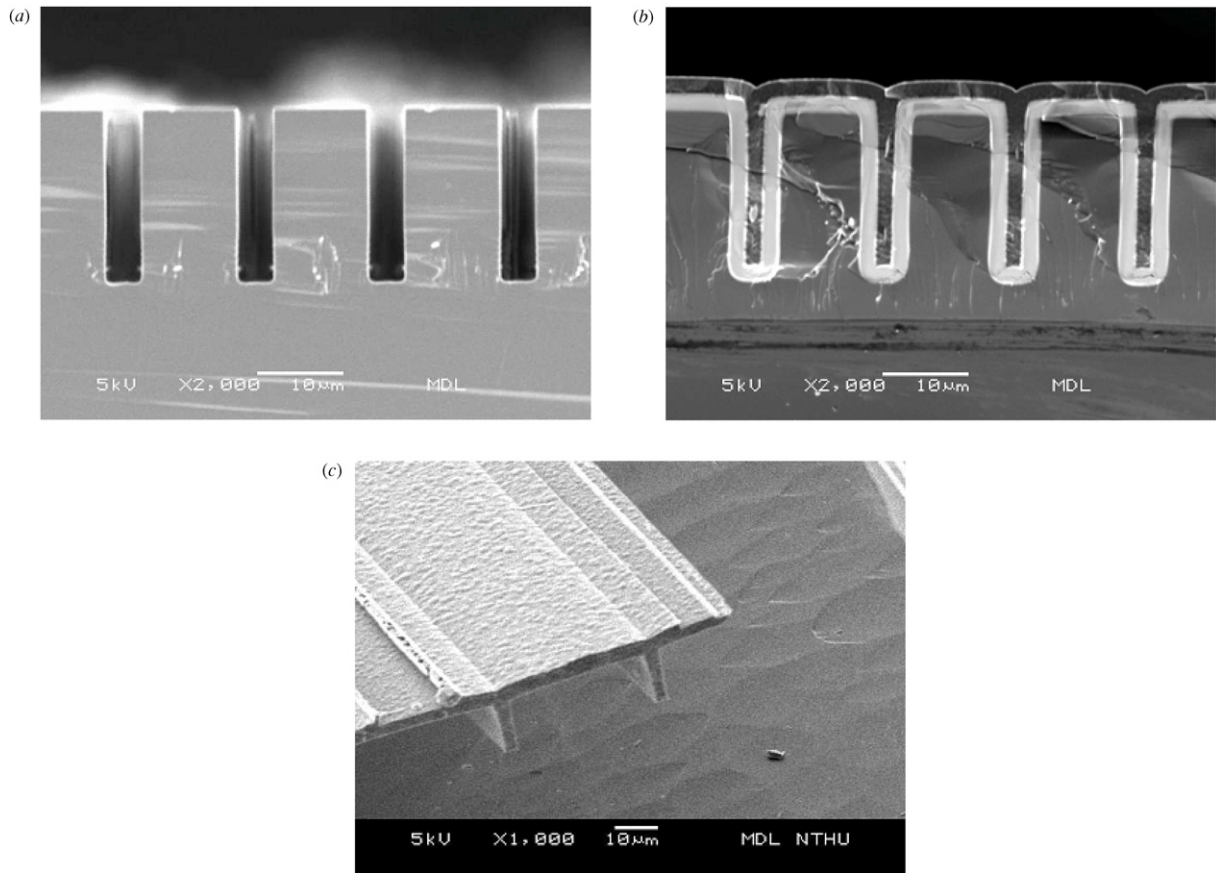


Figure 2. The SEM photos of the formation of trench-refilled structure: (a) the cross-section view of the 20 μm trenches, (b) the fully refilled 20 μm trenches, and (c) the trench-refilled structure after being released.

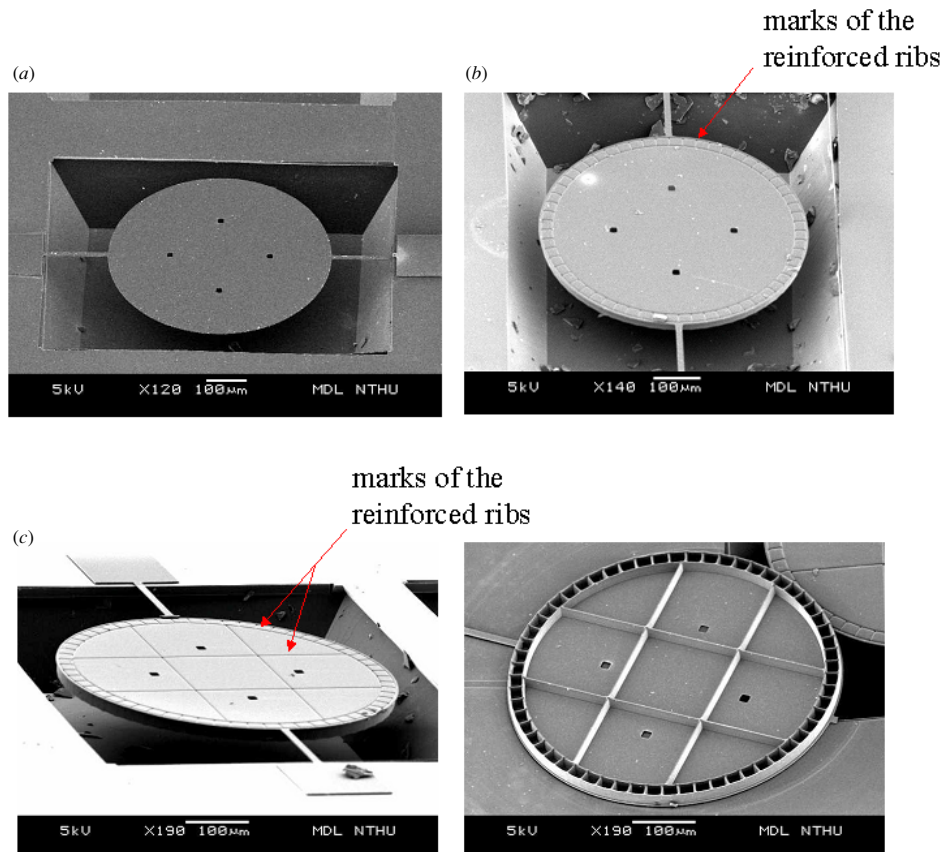


Figure 3. The SEM photos of the test circular mirror plates (a) without reinforced ribs, (b) with double-ring-type reinforced ribs on the boundary, and (c) with double-ring-type ribs on the boundary and grid-type ribs on the domain.

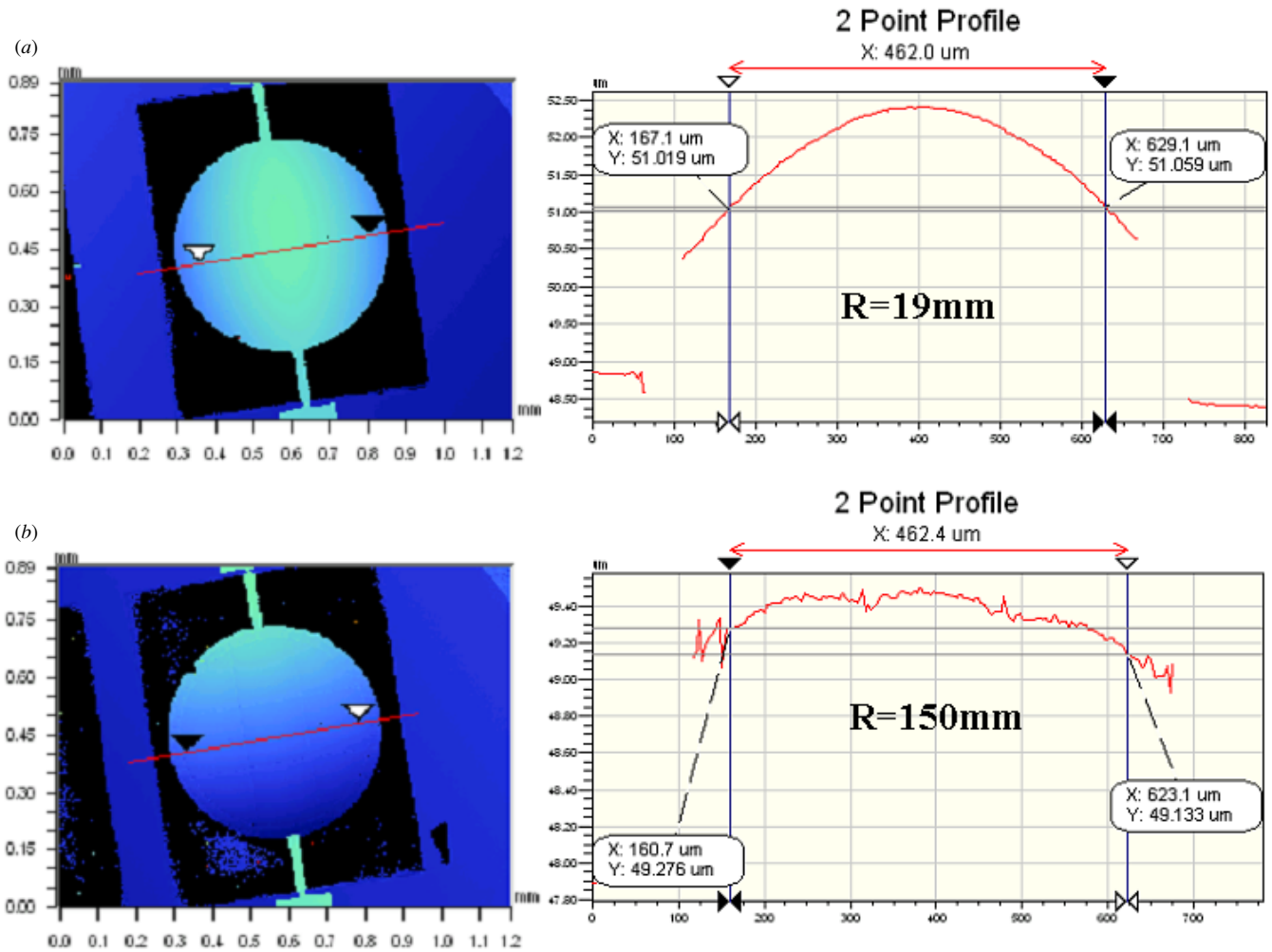


Figure 4. The ROC of the plates measured by optical interferometer (a) 19 mm, without reinforced ribs (in figures 3(a)) and (b) 150 mm, with reinforced double-ring and grid ribs (in figure 3(c)).

define the location of deeper trenches, as shown in figure 1(a). The photo resist in figure 1(a) was removed after the first DRIE. The silicon oxide acted as the etching mask for the second DRIE. The silicon substrate had trenches with two different depths after the second DRIE, as shown in figure 1(b). After that, these trenches were fully refilled by thermal oxide and first LPCVD (low pressure chemical vapor deposition) poly-Si films, as shown in figure 1(c). After the first poly-Si was patterned, the Si_xN_y sacrificial layer and second poly-Si structural layer were deposited and patterned, as shown in figure 1(d). The Si_xN_y and second poly-Si were also served as electrical interconnections. After being patterned with photo resist, the third DRIE was exploited to etch the first poly-Si, as shown in figure 1(e). The thickness of the trench-refilled poly-Si was trimmed, hence the micromachined structures located at different vertical positions became available. In figures 1(f)–(g), the low stress nitride was deposited and patterned as the etching mask for bulk silicon etching. Meanwhile, the poly-Si film was fully covered by the thermal oxide and the Si_xN_y films. The substrate was then immersed into TMAH solution for bulk silicon etching. The thermal oxide and the Si_xN_y performed as passivation layers for the poly-Si structure during bulk silicon etching. Finally, the passivation layers were removed by HF and the poly-Si structure was fully suspended, as shown in figure 1(h).

2.1. Thick and multi-depth structures by trench-refilled poly-Si

The performances of MEMS devices can be improved by tuning the thickness and the vertical position of the micromachined structures. For instance, the stiffness of the micromachined structures is significantly increased by tuning the film thickness. Moreover, the performance of the vertical comb actuator is improved by varying the vertical position of the electrodes [15]. This study employed the trench-refilled molding processes [13, 14] to tune the thickness and the vertical position of the micromachined structures.

The etching rate depends on the width of the trench opening. In this work, the width of the trench openings in figure 1(b) is designed to be a constant value ($4 \mu\text{m}$) for the whole wafer, so that the DRIE etching rate is a constant for different trenches. Figure 2(a) shows a typical cross-section view of the trenches with $20 \mu\text{m}$ in depth. Since the present MOSBE II process was fully compatible with the MUMPs process, the LPCVD poly-Si and thermal oxide layers in figure 1(c) were $2 \mu\text{m}$ thick. In this regard, the maximum trench width was $4 \mu\text{m}$ in order to be fully refilled by the poly-Si and sacrificial oxide layers [14]. As shown in figure 2(b), the $20 \mu\text{m}$ deep trench was fully refilled by thermal oxide and poly-Si. Consequently, the reinforced rib to increase the stiffness of the thin-film structures was realized. The SEM

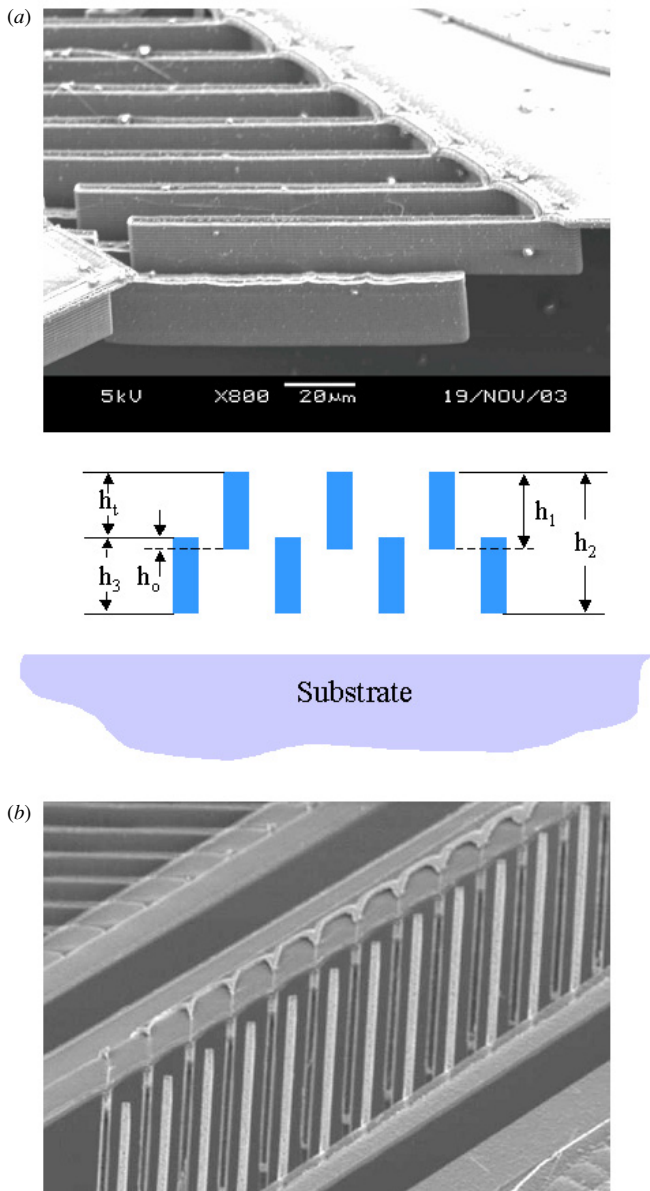


Figure 5. The SEM photos of the multi-depth structure (vertical comb electrodes), (a) bird's eye view and (b) top view.

photo in figure 2(c) shows a typical rib-reinforced beam after being released from the substrate. In this regard, the present processes were not only providing $2\ \mu\text{m}$ thick flexible thin-film structures but also offering stiff rib-reinforced structures. The influence and performance of the reinforced structures has been evaluated using the test circular plates with four different designs, as shown in figure 3. All of these three poly-Si circular plates were $2\ \mu\text{m}$ thick and $500\ \mu\text{m}$ in diameter. The circular plate in figure 3(a) had no reinforced ribs. On the other hand, the circular plate in figure 3(b) has double-ring type reinforced ribs on its boundary. In addition, the circular plate in figure 3(c) has double-ring-type ribs on its boundary and grid-type ribs on its domain. The right SEM photo of figure 3(c) shows the reinforced ribs at the backside of the plate. The reinforced ribs at the backside of the structure left a mark on the front side of them. These marks can be observed on the SEM photos of figures 3(b) and (c). The test circular plate in figure 3 was bent by the residual stress gradient. The optical interferometer was employed to measure the radius of

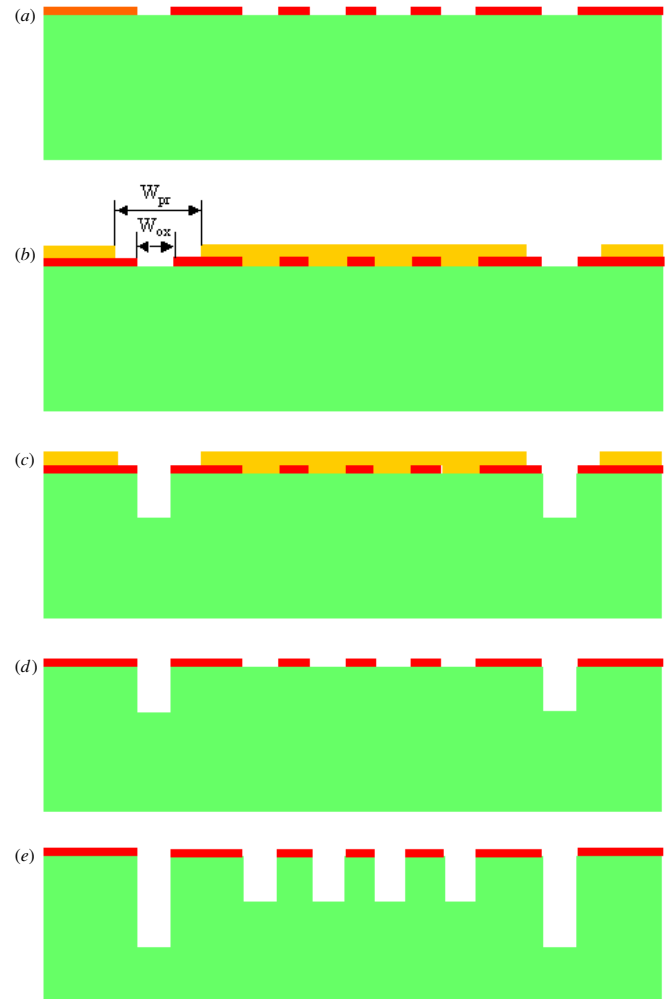


Figure 6. The detailed process steps of the two-step self-aligned DRIE etching technique.

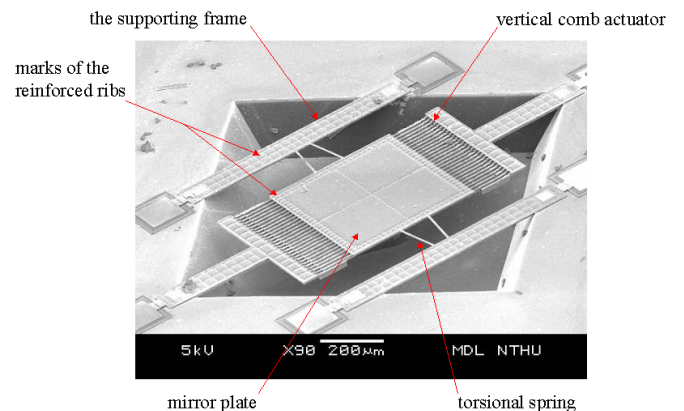


Figure 7. The optical scanner fabricated using the present process.

curvature (ROC) of these plates. Figures 4(a) and (b) show the typical measurement results of the ROC for the plates in figures 3(a) and (c), respectively. The ROC of the circular plate in figure 3(a) was $19\ \text{mm}$. After being stiffened by the reinforced ribs, the ROC of the plates in figures 3(b) and (c) became $92\ \text{mm}$ and $150\ \text{mm}$, respectively. Thus, the trench-refilled reinforced structure could significantly increase the stiffness of thin-film structure.

The vertical positions of micromachined structures were tunable using the DRIE trimming process, as indicated in

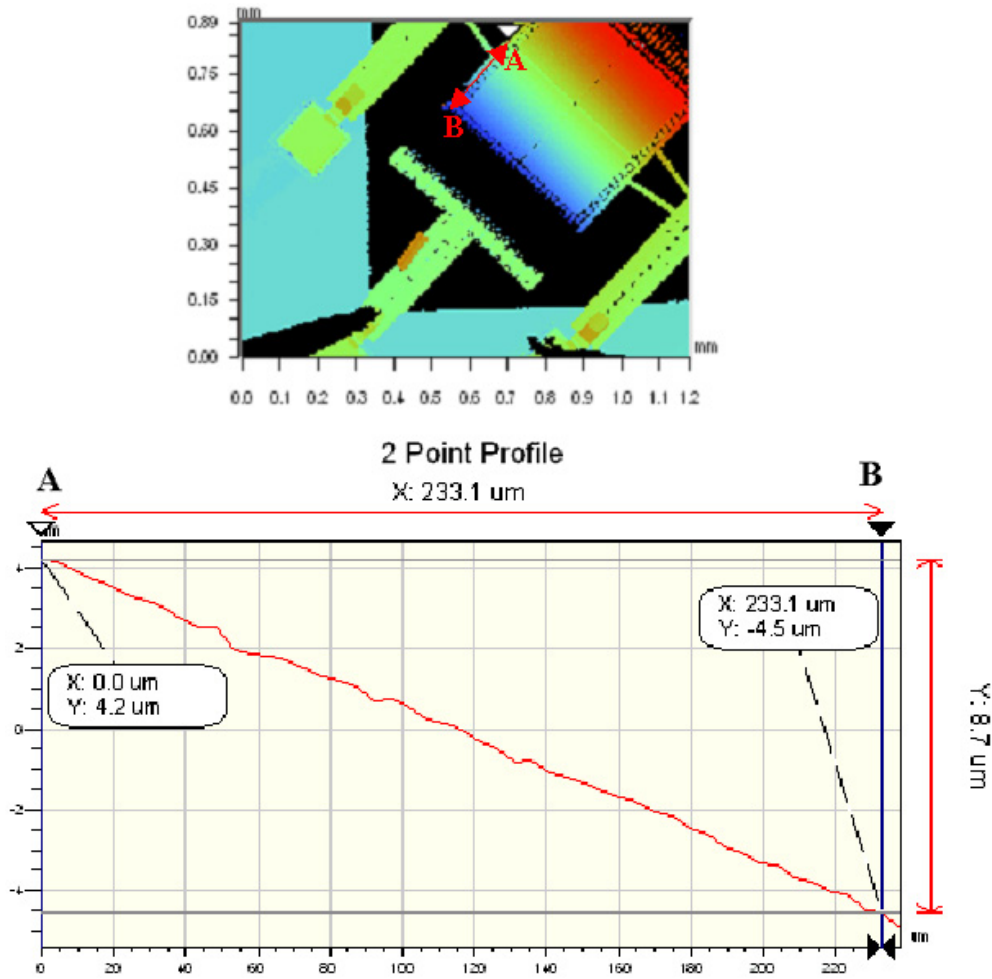


Figure 8. The deformation profile of the mirror measured by optical interferometer during static load-deflection test.

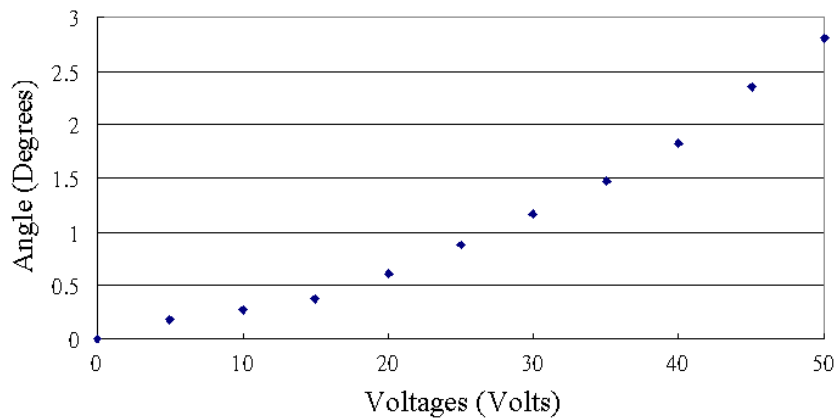


Figure 9. Variation of the driving voltage and the angular displacement of the mirror.

figure 1(e). This characteristic has various applications. For instance, the driving voltage and the traveling distance of vertical comb actuator can be improved. The SEM photo in figure 5(a) shows typical vertical comb electrodes fabricated using the presented approach. The schematic illustration shows the side view of these electrodes. The thicknesses h_1 and h_2 were defined by the depth of the trenches in figure 1(b). In addition, the initial overlap of the electrodes h_0 and the thickness h_3 of the electrode were tuned by the DRIE trimming

depth h_t in figure 1(e). The trimming depth h_t in figure 5(a) was $15 \mu\text{m}$.

2.2. Two-step self-aligned DRIE etching

In many applications, the alignment of the micromachined structures located at different vertical positions, such as vertical comb electrodes, is a critical issue. For instance, the vertical comb actuator may experience the fatal side-sticking effect if the misalignment of the electrodes occurred [16].

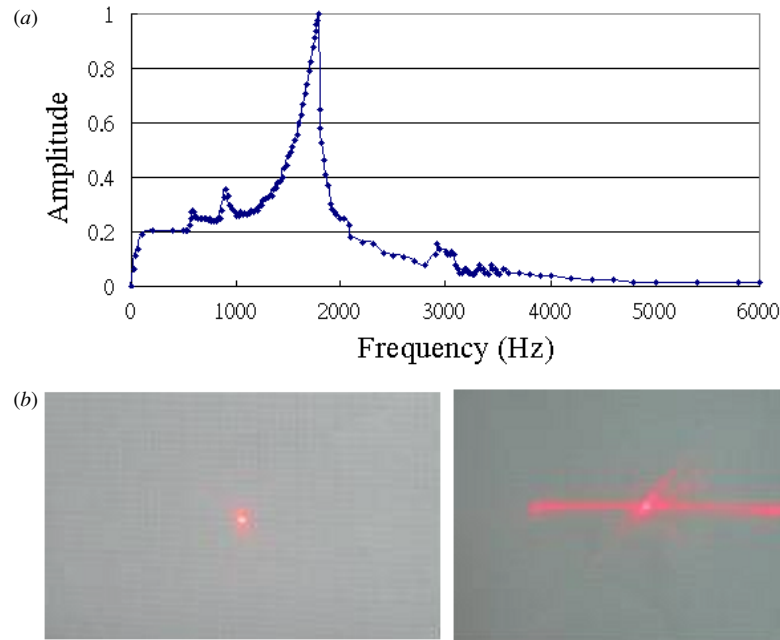


Figure 10. The experiment results for dynamic test: (a) frequency response and (b) laser scanning pattern.

This study presented a two-step self-aligned DRIE etching technique in figures 1(a) and (b) to implement these perfectly aligned trenches for various etching depths. The detailed fabrication steps are illustrated in figure 6. First, a thermal oxide was grown and patterned by the first photo mask. This mask was used to define the shape of both deep and shallow trenches simultaneously, as shown in figure 6(a). Next, the photoresist was spin on wafer and patterned by the second mask, as illustrated in figure 6(b). This step was used to select the location of the deep trench. As shown in figure 6(c), the first DRIE was employed to define a preliminary depth of these deep trenches. It is obtained from figure 6(c) that the shape of the deep trench was not defined by the photo resist but defined by the thermal oxide. As shown in figure 6(b), the purpose of the opening W_{pr} on photo resist was to allow the opening W_{ox} expose to the first DRIE. To this end, it was not required to perfectly align the openings W_{pr} and W_{ox} . Moreover the design had $W_{pr} \gg W_{ox}$, hence, the alignment tolerance became less critical in the process. As shown in figures 6(d) and (e), the photo resist was removed and then the substrate experienced the second DRIE etching. Therefore, the trenches with two different depths were precisely aligned. In other words, the structures formed using the trench-refilled process were also precisely aligned, as the comb electrodes shown in figure 5(b).

3. Applications

In application, the optical scanner in figure 7 was employed to demonstrate the capabilities of the MOSBE II process to fabricate and integrate the micromachined poly-Si structures with (1) various thickness and stiffness, (2) multi-depth and (3) bulk etching cavity. As indicated in figure 7, the scanner consists of the vertical comb actuator, the torsional spring, the mirror plate and the supporting frame. It is also clearly observed from the SEM photo that the scanner was suspended above a bulk micromachined cavity. Briefly, the mirror plate

was connected to two supporting frames by two torsional springs, and was designed to be driven by vertical comb actuators.

The cavity was available through the process to allow a large out-of-plane angular motion of the mirror plate. Apparently, no complicated assembly means and lifting structures were required. In order to integrate with the MUMP's process, components of the scanner in figure 7 were formed by two LPCVD poly-Si films ($1.5 \mu\text{m}$ and $2 \mu\text{m}$ thick). Thus, the $2 \mu\text{m}$ thick torsional bar was easily to be twisted to reduce the driving voltage. However, the $2 \mu\text{m}$ thick mirror plate and frames was not stiff enough to prevent the unwanted deformation by inertia force during operation and residual stresses after fabrication. This study employed $20 \mu\text{m}$ thick trench-refilled reinforced ribs shown in figure 2(c) to increase the stiffness of the mirror plate and supporting frame. The marks resulted from the reinforced ribs can also be clearly observed on the SEM photo of figure 7. The SEM photos in figure 5 show the close-up of the comb electrodes after bulk etching. The driving voltage of the vertical comb actuator depends on the initial overlap h_0 of the comb electrodes in figure 5(a) [15]. The electrostatic force of the actuator will reach a maximum at the position when the initial overlap h_0 is near zero. The driving force remains a constant when the initial overlap h_0 is between zero and $h_i/2$ ($i = 1$ if $h_3 > h_1$, and $i = 3$ if $h_1 > h_3$). Hence, it was important to tune the initial overlap h_0 during the DRIE trimming for the present scanner. In this study, the thickness of comb electrodes h_1 and h_3 were $20 \mu\text{m}$ and $25 \mu\text{m}$. The initial overlap of the electrodes h_0 was $5 \mu\text{m}$ which provided a large initial driving force to the scanner. The vertical comb electrodes, as demonstrated in figure 5(b), were self-aligned perfectly. Thus the side-sticking problem was reduced. Consequently, the optical scanner in figure 7 shows that the present processes have the capability of fabricate and integrate the micromachined devices with the aforementioned three characteristics.

To demonstrate the performance of the fabricated devices, the static and dynamic characteristics of the torsional mirror

plate in figure 7 were measured. During the static load-deflection test, the mirror plate was driven by dc voltages. The out-of-plane angular displacement of the mirror plate was measured by the optical interferometer. A typical measured result is shown in figure 8. The angular displacement of the mirror plate was $8.7 \mu\text{m}$ when the driving voltage was 42 V. Figure 9 shows the variation of the driving voltage and the angular displacement. According to the results, the mirror plate had a maximum scanning angle of 2.8° at 50 V. Thus, the total optical scanning angle of the scanner was 11.2° . In this case, the instability of vertical comb electrodes due to side-sticking can be reduced by the V-shape torsional bar [5]. Regarding to the dynamic scanning test, the optical scanner was driven by the vertical comb actuator using ac voltages (4 V peak-to-peak). The optical laser Doppler vibrometer was used to measure the dynamic response of the scanner. A typical frequency response is shown in figure 10(a), and the first resonant frequency which associated with the scanning mode is 1.8 kHz. The trace of the reflected laser spot from the scanner was shown in figure 10(b). The left photo shows the reflected laser spot when the mirror was stationary. The right photo shows the reflected laser spot when the scanner was driven at the first torsional mode.

4. Discussions and conclusions

The present MOSBE II process integrates multi-depth DRIE etching, trench-refilled molding, two-poly MUMPs and bulk releasing to accomplish superior poly-Si micro devices. This process offers the opportunity to fabricate thin-film devices with out-of-plane characteristic lengths ranging from $\sim 1 \mu\text{m}$ to $\sim 100 \mu\text{m}$. For instance, the flexible thin-film structure is $\sim 1 \mu\text{m}$ thick. The depth difference of the trench-refilled structures, such as vertical comb electrodes and the reinforced ribs, are in the range of 20–40 μm to increase the devices stroke and structure stiffness, respectively. Moreover, bulk Si etching creates a cavity ($> 100 \mu\text{m}$) that provides a moving space for micro components. The optical scanner driven by vertical comb actuators were realized to demonstrate the concept of this study. For instance, the stiffness of the structures was significantly increased by reinforced ribs, so that the radius of curvature of the $2 \mu\text{m}$ thick mirror even reached 150 mm. As a comparison, the $2 \mu\text{m}$ thick poly-Si mirror in [1] has a ROC of 18 mm, and a $22.5 \mu\text{m}$ thick SOI mirror has a ROC of 265 mm. The scanning angle of one-axis mirror is $\pm 2.8^\circ$ under 50 V dc voltages and the resonant frequency is 1.8 kHz. As a comparison, the optical scanning angle of the mirror in [17] is $\pm 1.8^\circ$ provided with a 110 V dc voltages. These poly-Si micro-optical devices can further integrate with the well-known MUMPs process to establish a more powerful MOEMS platform.

Acknowledgments

This project was (partially) supported by Ministry of Economic Affairs, Taiwan under contract no. 92-EC-17-A-07-S1-0011.

The authors would like to appreciate the National Science Council Central Regional MEMS Research Center (Taiwan), Nano Facility Center of National Chiao-Tung University (Taiwan), National Nano Device Laboratory (Taiwan) and Walsin Linwa Corp. (Taiwan) in providing the fabrication facilities.

References

- [1] Su G-D J, Nguyen H, Paterson P, Toshiyoshi H and Wu M C 2001 Surface-micromachined 2-D optical scanners with high-performance single-crystalline silicon micromirrors *IEEE Photonics Technol. Lett.* **13** 606–8
- [2] Milanovic V, Last M and Pister K S J 2001 Torsional micromirrors with lateral actuators *Transducers '01 (Munich, Germany, June, 2001)* pp 1298–301
- [3] Wu M C 1997 Micromachining for optical and optoelectronic systems *Proc. IEEE* **85** 1833–56
- [4] Bustillo J M, Howe R T and Muller R S 1998 Surface micromachining for microelectromechanical systems *Proc. IEEE* **86** 1552–74
- [5] Milanović V 2004 Multilevel-beam SOI-MEMS fabrication and applications *J. Microelectromech. Syst.* **13** 19–30
- [6] Lin L-Y, Goldstein E L and Tkach R W 2000 On the expandability of free-space micromachined optical cross connects *J. Lightwave Technol.* **18** 482–8
- [7] Lin H-Y, Wu M-C, Tsai M-L and Fang W 2001 Towards a lightwave MEMS platform using MOSBE process *IEEE/LEOS Optical MEMS (Okinawa, Japan, Aug., 2001)* pp 27–8
- [8] Lin H-Y and Fang W 2003 A reinforced micro-torsional-mirror driven by electrostatic torque generators *Sensors Actuators A* **105** 1–9
- [9] Helmbrecht M A, Srinivasan U, Rembe C, Howe R T and Muller R S 2001 Micromirrors for adaptive-optics arrays *Transducers '01 (Munich, Germany, June, 2001)* pp 1290–3
- [10] Aksyuk V A, Pardo F and Bishop D J 1999 Stress-induced curvature engineering in surface-micromachined devices *Proc. SPIE* **3680** 984–93
- [11] Ho Y-P, Wu M, Lin H-Y and Fang W 2002 A robust and reliable stress-induced self-assembly mechanism for optical devices *IEEE/LEOS Optical MEMS (Lugano, Switzerland, Sept., 2002)* pp 131–2
- [12] Fan L and Wu M C 1998 Two-dimensional optical scanner with large angular rotation realized by self-assembled micro-elevator *IEEE/LEOS Summer Topical Meeting (Monterey, CA, July, 1998)* pp 107–8
- [13] Keller C G and Howe R T 1997 HexSil tweezers for teleoperated micro-assembly *MEMS'97 (Nagoya, Japan, Jan., 1997)* pp 72–7
- [14] Ayazi F and Najafi K 2000 High aspect-ratio combined poly and single-crystal silicon (HARPSS) MEMS technology *J. Microelectromech. Syst.* **9** 288–94
- [15] Tsai J M-L, Chu H-Y, Hsieh J and Fang W 2004 The BELST II process for silicon HARM vertical comb actuator and its applications *J. Micromech. Microeng.* **14** 235–41
- [16] Tsuboi O, Mizuno Y, Koma N, Soneda H, Okuda H, Ueda S, Sawaki I and Yamagishi F 2002 A rotational comb-driven micromirror with a large deflection angle and low drive voltage *IEEE MEMS'02 (Las Vegas, NV, Jan., 2002)* pp 532–5
- [17] Patterson P R, Hah D, Nguyen H, Toshiyoshi H, Chao R-M and Wu M C 2002 A scanning micromirror with angular comb drive actuation *IEEE MEMS'02 (Las Vegas, NV, Jan., 2002)* pp 544–7

Queries

- (1) Author: Please be aware that the colour figures in this article will only appear in colour in the Web version. If you require colour in the printed journal and have not previously arranged it, please contact the Production Editor now.